

Formation and Evolution of Planetary Systems: Upper Limits to the Gas Mass in HD 105

D.Hollenbach¹, U.Gorti², M.Meyer³, J.S.Kim³, P.Morris⁴, J.Najita⁵, I.Pascucci³, J.Carpenter⁶, J.Rodmann⁷, T.Brooke⁶, L.Hillenbrand⁶, E.Mamajek⁸, D.Padgett⁴, D.Soderblom⁹, S.Wolf⁷, J.Lunine¹⁰

ABSTRACT

We report infrared spectroscopic observations of HD 105, a nearby (~ 40 pc) and relatively young (~ 30 Myr) G0 star with excess infrared continuum emission, which has been modeled as arising from an optically thin circumstellar dust disk with an inner hole of size $\gtrsim 13$ AU. We have used the high spectral resolution mode of the Infrared Spectrometer (IRS) on the Spitzer Space Telescope to search for gas emission lines from the disk. The observations reported here provide upper limits to the fluxes of H₂ S(0) 28 μ m, H₂ S(1) 17 μ m, H₂ S(2) 12 μ m, [FeII] 26 μ m, [SiII] 35 μ m, and [SI] 25 μ m infrared emission lines. The H₂ line upper limits directly place constraints on the mass of warm molecular gas in the disk: $M(\text{H}_2) < 4.6, 3.8 \times 10^{-2},$ and $3.0 \times 10^{-3} M_J$ at $T = 50, 100,$ and 200 K, respectively. We also compare the line flux upper limits to predictions from detailed thermal/chemical models of various gas distributions in the disk. These comparisons indicate that if the gas distribution has an inner hole with radius $r_{i,gas}$, the surface density at that inner radius is limited to values ranging from $\lesssim 3 \text{ gm cm}^{-2}$ at $r_{i,gas} = 0.5$ AU to 0.1 gm cm^{-2} at $r_{i,gas} = 5 - 20$ AU. These

¹NASA Ames Research Center, Moffett Field, CA 94035

²University of California, Berkeley, CA 94720

³Steward Observatory, The University of Arizona, Tucson, AZ 85721

⁴Spitzer Science Center, California Institute of Technology, Pasadena, CA 91125

⁵National Optical Astronomy Observatory, Tucson, AZ 85719

⁶California Institute of Technology, Pasadena, CA 91125

⁷Max-Planck-Institut für Astronomie, Heidelberg, Germany

⁸Harvard-Smithsonian Center for Astrophysics, Cambridge, MA 02138

⁹Space Telescope Science Institute, Baltimore, MD 21218

¹⁰Lunar Planetary Laboratory, The University of Arizona, Tucson, AZ 85721

values are considerably below the value for a minimum mass solar nebula, and suggest that less than $1 M_J$ of gas (at any temperature) exists in the 1 – 40 AU planet-forming region. Therefore, it is unlikely that there is sufficient gas for gas giant planet formation to occur in HD 105 at this time.

Subject headings: planetary systems:formation—stars:individual (HD105) — infrared:stars — solar system:formation

1. Introduction

Observations of young stars indicate that circumstellar disks of gas and dust are common in the earliest stages of evolution (e.g., Beckwith & Sargent 1996, Hillenbrand et al. 1998, Haisch et al. 2001, Weinberger et al. 2004, Natta et al. 2004). Most of these studies rely on infrared, submillimeter, or millimeter wavelength emission as the signature of small ($\lesssim 1$ mm) warm dust particles, which trace only a small fraction of the circumstellar gas and solid particles. In their initial active accretion phase, circumstellar disks are composed of primordial molecular cloud material, possibly somewhat processed by the collapse through the accretion shock onto the disk, with gaseous hydrogen and helium constituting 99% of the total mass and with $\sim 1\%$ of the disk mass in small dust particles. As infall from the cloud onto the star+disk system diminishes, the gas and dust components of the disk evolve, presumably losing most of the gas via accretion onto the central star or photoevaporation back to the interstellar medium (Hollenbach et al. 1994, Johnstone et al. 1998, Clarke et al. 2001, Adams et al. 2004). Some of the small dust grains presumably coagulate, growing to eventually form planetesimals and rock/ice planets (e.g., Pollack et al. 1996, Weidenschilling 1977, 1997). During these processes, the circumstellar disk undergoes a transition from being optically thick and (mostly) gaseous to becoming optically thin and (mostly) dusty. There have been many theoretical and observational studies of disks in various stages of evolution pointing towards such a sequence (e.g., Weidenschilling 1997, Suttner & Yorke 2001, Throop et al. 2001, Przygodda et al. 2003, Hogerheijde et al. 2003, Testi et al. 2003, van Boekel et al. 2003, Wolf et al. 2003, Dullemond & Dominik 2004, Kessler-Silacci et al. 2005). Such studies have, however, concentrated only on the more readily observed dust emission from the disk, and suggest the evolution of dust to larger particle sizes and hence lower opacity (Miyake and Nakagawa, 1993).

Observations of gas and its evolution are in their infancy. Most studies to date have probed either at near infrared wavelengths (often CO vibrational transitions) the very hot inner surface regions less than about 1 AU from the star (Carr, Mathieu & Najita 2001, Brittain et al. 2003, Najita et al. 2003, Blake & Boogert 2004, Rettig et al. 2004, Thi et

al. 2005), or at millimeter wavelengths (often CO rotational transitions) extended gas-rich disks that are hundreds of AU in size (e.g., Skrutskie et al. 1991, Zuckerman et al. 1995, Dutrey et al. 1998, Duvert et al. 2000, Pietu et al. 2003, Qi et al. 2003, , Dent et al. 2005, Greaves 2005). The millimeter observations are generally not sensitive to gas at $\lesssim 30$ AU because the lines become beam-diluted and weak. In addition, the trace species used as millimeter wavelength probes of gas may freeze out onto grain surfaces at $\gtrsim 30$ AU, making these observations somewhat unreliable for estimating gas masses (e.g., van Dishoeck 2004).

The presence or absence of gas in the planet-forming 1–30 AU regions is difficult to constrain from observations in the near infrared or at millimeter wavelengths. Temperatures in these regions may range from 300–50 K, and warm gas emitting at these temperatures is best probed in the mid-infrared lines of H₂ at 28.2 and 17.0 μm , and the mid-infrared fine structure lines of abundant ions and atoms, like [SI] 25.2 μm (Gorti & Hollenbach 2004, hereafter GH04). These lines are difficult or impossible to observe from the ground. Furthermore, the strong dust continuum of very young objects makes the line to continuum ratio quite low, and the background noise high, unless the lines are spectroscopically resolved (requiring resolving powers from 30,000–100,000). The Infrared Space Observatory (ISO) provided some tantalizing evidence for long-lived gas-rich disks by observing mid-infrared emission lines of H₂ toward debris disk candidates (Thi et al. 2001). However, ground-based observations (Richter et al. 2002, Sheret et al. 2003, Sako et al. 2005), FUSE results (LeCavalier des Etangs et al. 2001), and Spitzer observations (Chen et al 2004) have called some of these results into question. Recently, ground-based IR and space-based UV observations have detected rovibrational (e.g., Bary et al. 2003) and fluorescent (e.g., Herczeg et al. 2002) H₂ emission towards young disks. The fluorescent H₂ emission is found to occur from gas that is warm and probably located within a few AU of the star. The narrow linewidths of the rovibrational IR emission suggests that the emission occurs at much larger distances from the star (>10 AU), and arises either from non-thermal UV pumping or from the X-ray heating of a very small amount of H₂ gas located in the low-density upper atmosphere. The likely non-thermal excitation of the H₂ seen both in the IR and UV makes it difficult to convert the detected line strengths into gas masses.

The nature of gas and dust evolution in circumstellar disks is an intriguing problem for various reasons. A determination of the gas dispersal timescales is important for understanding the formation of planetary systems, and specifically for discriminating between the two competing theories that exist for gas giant planet formation. Core accretion theories for forming gas giants (e.g. Lissauer et al. 1993, Pollack et al. 1996, Kornet et al. 2002, Hubickyj, Bodenheimer, & Lissauer 2004) require long ($\gtrsim 1$ Myr) gas disk lifetimes to facilitate the formation of rocky cores of a few Earth masses and their subsequent gas accretion to form planets. Detection of gas in older ($\sim 3 \times 10^6$ year) disks would help validate the efficacy

of this scenario. The alternate theory of gravitational instability in disks (e.g., Boss 2003) allows the formation of gas giants quickly and the gas may dissipate rapidly. The presence of small amounts of gas in the “terrestrial” zone, 0.1 – 5 AU, in later evolutionary stages (~ 10 Myrs) influences the dynamics of the smaller planets and planetesimals and is decisive in the final outcome of the planetary system (Agnor & Ward 2002; Kominami & Ida 2002, 2004). Only a narrow range of gas masses ($\sim 0.01 M_J$) in this stage of terrestrial planet formation allow for the formation of an Earth-sized planet in an orbit as circular as the Earth. At even later stages ($> 10^7$ years) in disk evolution, small masses of gas ($\sim 0.01 M_J$) can affect dust dynamics via drag forces and hence significantly influence disk structure (Klahr & Lin 2001, Takeuchi & Artymowicz 2001, Takeuchi & Lin 2002), weakening interpretations of gaps and ring signatures as being due to the presence of planets.

This paper highlights the potential of the recently launched Spitzer Space Telescope in detecting small amounts of gas (or setting stringent limits on gas mass) in the planet-forming regions of disks around nearby young stars. The Spitzer Space Telescope is able to observe the thermal emission from deep layers in the planet-forming zone, sampling significant mass in this 0.3–30 AU intermediate zone inaccessible to most other techniques. Gas in these regions is likely to be warm (~ 100 K) and line emission at the mid-infrared (10 – 37 μ m) wavelengths seen by the Spitzer Infrared Spectrometer (IRS) instrument can probe total gas masses as small as $\sim 0.01 M_J$ in the inner (< 20 AU) regions around nearby ($\lesssim 30$ pc) stars (GH04). Gas line diagnostics in the Spitzer band include the S(0), S(1) and S(2) pure rotational lines of H₂, atomic fine structure lines of [SI], [FeI], [SiII], [FeII] and molecular lines of OH and H₂O (GH04).

The Formation and Evolution of Planetary Systems (FEPS) Spitzer Legacy Science Project (Meyer et al 2005) aims to study the evolution of gas in disks by targeting a carefully chosen sample of about 40 nearby solar-type stars for high resolution ($R \simeq 700$) spectroscopic observations by the IRS (Houck et al. 2004). The sample was selected mainly on the criteria that they span an age range of 3-100 Myr, and that they be nearby (< 140 pc) so that the expected weak line fluxes may be detectable with the IRS. A secondary criterion was that they show some infrared excess emission indicative of the presence of dusty disks. To some extent, we favored sources with strong X ray luminosities, since the X rays heat the putative gas and intensify the resultant line luminosities. This will be the most comprehensive survey to date of gas in transition and post-accretion systems in order to characterize its dissipation and to place limits on the time available for giant planet formation.

In this paper, we present high resolution IRS data and detailed modeling results for one of the first sources observed through the FEPS gas program, HD 105. HD 105 is a young (~ 30 Myr) solar-type star 40 pc from the Sun with an infrared excess indicative of

a dust disk (Meyer et al. 2004). The star has completed its active accretion phase and the dust continuum is characteristic of an optically thin, debris disk. The youth and proximity of the star, the presence of dust (which may imply associated gas), the relatively low dust continuum luminosity that allows the detection of weak gas lines, and the presence of X-ray flux from the central star (a source of gas heating) make HD 105 a promising candidate for the detection of mid-infrared gas lines. *Spitzer spectroscopic observations of HD 105, however, did not detect any gas emission lines, but instead set stringent upper limits on the line fluxes.* The line flux upper limits are used to set limits on the gas surface density and mass in HD 105. Assuming that the gas distribution has an inner hole of radius $r_{i,gas}$ greater than about 0.5 AU, we find that there is very little gas in the disk beyond the inner hole, suggesting the end of the main planet-building epoch for gas giants in these regions.

Debris disks have been observed around early (e.g., 49 Cet, A1V) and late-type (e.g., AU Mic; MIV) stars and are often characterized by their fractional infrared luminosities, $f = L_{IR}/L_{bol}$, which range from $10^{-5} - 10^{-3}$. HD 105 is thus a somewhat luminous debris disk, with a fractional infrared luminosity, $f = L_{IR}/L_{bol} \sim 4 \times 10^{-4}$. The disk may have evolved past its main planet formation stage, and is young enough to perhaps be a “transition object” with some residual, detectable gas. Though gas is readily detected in young disks (ages \sim a few Myrs, and $f \gtrsim 0.01$, e.g. Dent et al. 2005), most debris disks do not appear to have detectable amounts of gas. Notable exceptions are the disks around 49 Cet ($f \sim 10^{-3}$) and β Pictoris ($f \sim 10^{-3}$). CO emission has been observed from the J= 3 \rightarrow 2 (Dent et al. 2005) and the J= 2 \rightarrow 1 (Zuckerman, Forveille & Kastner 1995) transitions from the disk around 49 Cet, and ISO detected H₂ 28 μ m emission as well (Thi et al. 2001). In β Pic gas emission from metal atoms and ions orbiting in a disk has been reported, most recently by Brandeker et al (2004). They and Thebault & Augereau (2005) derive gas masses in the disk of $\sim 0.1 - 0.4 M_{\oplus}$. This amount of gas is insufficient to brake the ions against radiation pressure; both groups estimate $\sim 40 M_{\oplus}$ is needed for braking. Chen et al. (2004) obtain upper limits on *warm* gas in β Pic of about 11 M_{\oplus} , although these Spitzer observations of the pure rotational lines of H₂ are not sensitive to the presence of cold (< 50 K) or atomic gas. The directly detected gas suggests gas depletion in debris disks relative to the dust, in the few instances where gas has been observed. HD 105 is the first debris disk observed in our FEPS H₂ program aimed at studying gas dispersal in disks as they evolve. As we shall show below, depending on the gas temperature, Spitzer is able to detect gas masses $\gtrsim 1 - 10 M_{\oplus}$ for sources as close as HD 105.

The outline of the paper is as follows. We describe the source (§2), and discuss the analysis of the Spitzer observations (§3). We then describe the gas and dust disk modeling (§4). Our results are discussed in §5 and the summary and conclusions presented in §6.

2. Source Description

HD 105 is a G0 V spectral type star (Houk 1978) located at an Hipparcos distance of 40 ± 1 pc (Perryman et al 1997). Based on its observed space motion and corroborating age diagnostics, Mamajek et al. (2004) conclude that it is a likely member of the Tuc-Hor association. The membership suggests an age of about 30 Myr for HD 105. There are various other indicators of the young age of this dwarf: its Li I $\lambda 6707$ equivalent width (e.g. Cutispoto et al. 2002) is similar to the ~ 50 Myr-old members of the IC 2602 and 2391 clusters (Randich et al. 2001), and it is stronger than that of the 120 Myr-old Pleiades stars (Soderblom et al. 1990); HD 105 has an active chromosphere as revealed by the detection of Ca II H and K emission (Henry et al. 1996) and its X-ray luminosity ($L_X = 2.4 \times 10^{29}$ ergs s $^{-1}$) suggests youth (Metanomski et al. 1998, Wichmann et al. 2003). Based on all these age indications, we assigned an age of 30 ± 10 Myr for HD 105 (Meyer et al. 2004).

Early ISO observations showed that HD 105 displays infrared excess emission at 60 and 90 μm (Silverstone 2000). Our recent Spitzer measurements detect no excess emission at 24 μm , confirm the excess at 70 μm , and detect dust emission even at 160 μm (Meyer et al. 2004, hereafter M04). B. Mazin (private communication) reports a 3σ upper limit to the 350 μm continuum flux of 2.1 Jy. We have searched the GALEX database at the position of HD 105 and found a source offset from the HD 105 position by about $3.2''$ in the NUV, but only $0.09''$ in the FUV, whereas the typical positional uncertainty is about $1''$. However, there is no other GALEX source within $30''$ of HD 105. Figure 1 shows the Kurucz model SED and the observed SED, including the infrared, submillimeter, and GALEX data. As expected for a young star, the source has FUV excess. Meyer et al. (2004) presented early models of the dust distribution implied by the far infrared excesses. The lack of detectable excess emission at wavelengths shorter than 35 μm implies very little circumstellar dust in the inner ($\lesssim 15$ AU) disk. We discuss these early models and other possible model fits in §4.

3. Observations and Analysis

3.1. Observations and Data Reduction

We obtained 9.9 - 37.2 μm spectra of HD 105 on December 14, 2003 UT using the Infrared Spectrograph (IRS, Houck et al. 2004) onboard the Spitzer Space Telescope (Werner et al. 2004). The spectra we present here were obtained with the two echelle modules ($R = 700$) covering 9.9 - 19.5 μm with the Short High (SH) detector array, and 18.9 - 37.2 μm with the Long High (LH) array. We also acquired low resolution observations ($R = 80$), which were used to account for background flux levels (discussed below). The spectra were acquired

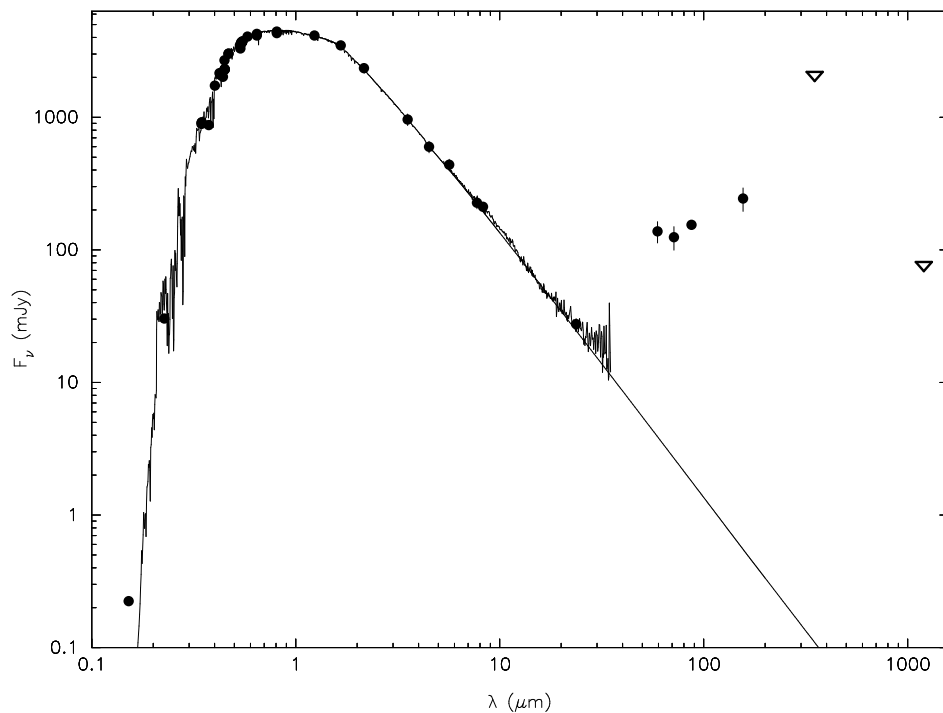


Fig. 1.— Observations and Kurucz model of HD 105. The solid curve through the observed fluxes is the best fit Kurucz model with $T_{eff} = 6063$ K, $A_V = 0.0$, and $\log g = 4.7$. Also shown are the ISO data at 60 and 90 μm (Silverstone 2000), our own Spitzer MIPS and low resolution IRS data (Meyer et al. 2004), GALEX data taken from its archive, a 350 μm upper limit provided by B. Mazin, and a 1 mm upper limit from Carpenter et al. (2005).

using the standard Staring Mode AOT, in which the telescope is nodded to place the star at two positions along each slit, resulting in four separate pointings (two for SH, and two for LH). For the SH observations, we used integration times of 31.5 seconds for each Data Collection Event (DCE), and cycled eight times for a total on-source exposure time of 504 seconds. For LH we used the 14.7 second integration time, also cycled eight times, for a total exposure time of 235 seconds. High accuracy blue peak up ($13.3 - 18.7\mu\text{m}$) was performed on the star to ensure a pointing accuracy within $0''.4$. The brightness profile of HD 105 in the peak up image agrees with that expected from the point spread function.

Individual DCEs were processed through the SSC pipeline (version S10.5.0) resulting in Basic Calibrated Data (BCD) products to which basic detector calibrations, dark current subtraction, cosmic ray detection, integration ramp fitting, and reduction to individual, two-dimensional slope images in units of electrons/second/pixel have been applied. Dark current measurements taken with the LH module within 12 hours of the HD 105 observations were used to mitigate the effects of outlier pixels whose dark currents vary on timescales of one to several days, rather than using standard dark current subtraction which employs darks taken over a wider separation in time.

The number of LH outlier pixels (high dark current pixels not representative of expected gaussian noise) is less than 6% of the 128×128 pixels on the array. However, they may dominate the noise within each echelle order if untreated. Corrections were applied to pixels flagged as anomalous in the pipeline, due to cosmic-ray saturation early in the integration, or having been preflagged as unresponsive. For these pixels we applied cubic spline interpolation technique, relying on 1.5 resolution elements on either side of the dead pixels in the dispersion direction. This signal reconstruction method has been successfully verified with observations of spectral standards exhibiting resolved and unresolved emission lines, particularly for the LH array.

Individual 1-dimensional spectra were extracted from two dimensional images flat-fielded with observations of the zodiacal background. We used the offline SSC software to extract these spectra using the full width of each echelle order. Spectral response and flux calibration corrections were applied to these 1-dimensional spectra. The response functions and flux calibration are based on similarly processed and spatially flatfielded observations of photometric standards HR 6688 (K2III), HR 6705 (K1.5III), HR 7310 (G9III), and HR 2194 (A0V), and the MARCS-code stellar atmosphere models tailored for these stars (Decin et al. 2004). The response correction of the short wavelength end of the SH data ($9.9 - 12.0\mu\text{m}$) of HD105 relied solely on HR 2194, in order to minimize any possible discrepancies in the strength of the SiO fundamental band in the K giants.

The 16 individual spectra for each module were next median combined on a spectral

order basis. Each order was trimmed, removing $\sim 5\%$ of the data at the blue ends where the throughput response of the arrays is lowest. The signal-to-noise in the continuum is lower than the signal-to-noise that would be inferred from repeatability among the 16 spectra. This suggests that the signal-to-noise is limited by residual errors due to fringing, uncertainty in the spectra response function and anomalous pixels among others. The errors in absolute fluxes, which here include both the star and zodiacal background, are thought to be $\sim 20\%$.

Although we did not obtain off-source exposures with SH or LH for sky subtraction, approximate corrections were applied, based on the background estimator available in the SPOT planning tool. These fluxes are provided in MJy/sr, which we then converted to Jy using the solid angles subtended by each of SH and LH apertures (1.25×10^{-9} sr and 5.82×10^{-9} sr, respectively). Since the SPOT background estimate is derived from measurements made with low spatial resolution, we also compared the extracted sky spectrum obtained with the IRS near HD 105 at low spectral resolution. We found agreement to within 20% of the fluxes provided by the background estimator between 15 and 40 μm when scaled by the appropriate solid angles.

Figure 2 shows the high resolution spectrum of HD 105. Figure 3 highlights the regions around the strongest emission lines expected from our models (Gorti & Hollenbach 2004). The S/N is approximately 12 in the 16 – 18 μm range, where the noise is computed as the $1\text{-}\sigma$ RMS spread in the ratio between the sky-subtracted IRS spectrum and the adopted Kurucz photospheric model over this essentially featureless region of the continuum (excluding the 16.9 – 17.1 μm range where we searched for evidence of the H₂ S(1) line). Similarly, we estimate a S/N ratio of approximately 10 in the 26.5 – 28.5 μm range. The S/N ratio becomes very low at $\lambda > 35\mu\text{m}$, where the LH throughput is at its lowest.

3.2. Analysis

To estimate upper limits of unresolved lines, we fit the spectrum using a Levenberg-Marquardt (LM) algorithm assuming a Gaussian for the line profile and a second order polynomial for the continuum. The central wavelength of the line was fixed in the fit, as was the width of the Gaussian to match the instrumental line profile. To fit the baseline locally, we used a wavelength range of $\pm 0.5\mu\text{m}$ centered on each feature (see Table 1). Five sigma upper limits to the line flux for each non-detection were derived taking the local RMS dispersion in the averaged continuum over two pixels per resolution element. We show examples of hypothetical 5σ lines in Figure 3. Several anomalous pixels are evident in the spectra (e.g. at 12.45 and 16.56 μm) that were not flagged in the data reduction discussed

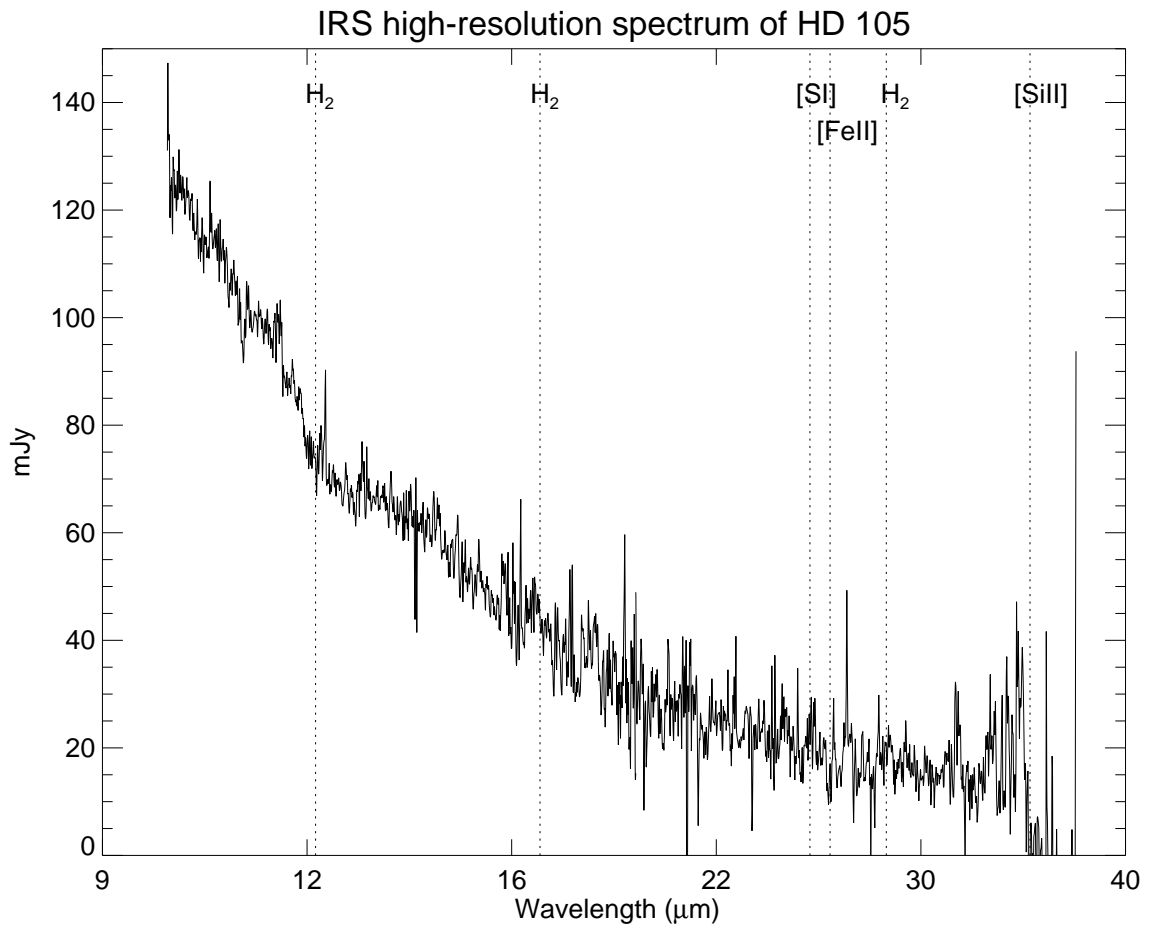


Fig. 2.— IRS spectrum of the $10\mu\text{m}$ to $38\mu\text{m}$ wavelength covered by SH and LH, the high resolution mode.

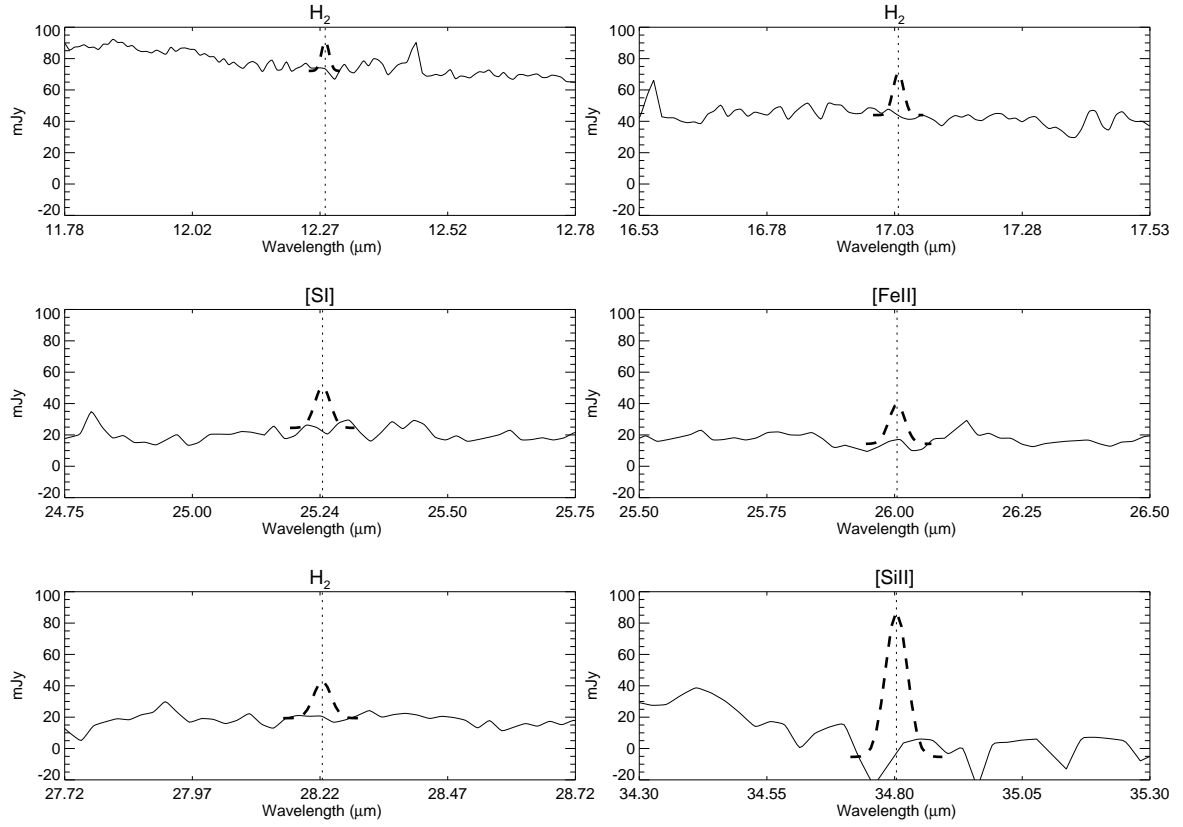


Fig. 3.— Expanded view of the wavelength regions around the expected strong lines. Also shown in dashed lines are the hypothetical 5σ line fluxes.

Table 1: Line flux upper limits obtained by Spitzer IRS High Resolution observations of HD105

Gas Species	Wavelength (μm)	Line flux upper limits (W/cm^2)
H ₂ S(2)	12.28	7.1×10^{-22}
H ₂ S(1)	17.035	7.2×10^{-22}
SI	25.249	4.7×10^{-22}
FeII	26.000	4.4×10^{-22}
H ₂ S(0)	28.221	3.8×10^{-22}
SiII	34.800	1.2×10^{-21}

in §3.1. Since these do not correspond to any expected emission lines, this suggests that residual systematic effects may be present in the spectra shown. Table 1 gives the upper limits to the line fluxes of H₂, [SI], [FeII], and [SiII] lines to estimate upper limits of gas mass in this system.

4. Modeling the Gas and Dust in the Disk Around HD105

4.1. Simple Estimate of the Upper Limit to Warm H₂ Mass

Before presenting detailed models of gas/dust disks around HD 105, which can provide estimates of upper limits to the *total* gas mass in atomic and molecular form and at a (model-determined) range of temperatures, we calculate here a simple upper limit to the warm H₂ mass assumed to be at a constant temperature T in the HD 105 disk. We use the upper limits on the H₂ S(0) 28 μm and S(1) 17 μm line fluxes to directly set limits on the mass of warm H₂ at temperature T in HD 105.

The H₂ S(0) and S(1) transitions have critical densities much lower than the gas densities in disks with gas masses $\gtrsim 3 \times 10^{-5} M_J$, the extreme lower limit for H₂ line detection by Spitzer of HD 105 or other sources at 40 pc (see below). Therefore, for any detectable disk or even for disks with H₂ masses somewhat below detectability, the lower rotational levels (i.e., J=0-3) of H₂ are in LTE.

With LTE and optically thin assumptions we calculate the mass $M(H_2)$ of molecular gas at temperature T and at the distance (40 pc) of HD 105 that will produce a line flux F for both the S(0) and S(1) transitions.

$$M(H_2) \simeq 2.8 \times 10^{-5} \left(\frac{F_{S(0)}}{10^{-22} \text{ Watts cm}^{-2}} \right) \left(1 + \frac{T}{85 \text{ K}} \right) e^{510 \text{ K}/T} M_J \quad (1)$$

$$M(H_2) \simeq 7.4 \times 10^{-7} \left(\frac{F_{S(1)}}{10^{-22} \text{ Watts cm}^{-2}} \right) \left(1 + \frac{T}{85 \text{ K}} \right) e^{1020 \text{ K}/T} M_J \quad (2)$$

Utilizing these equations and the upper limits for the line fluxes given in Table 1, we find upper limits on the H₂ gas mass of 4.6 M_J at 50 K, 3.8×10⁻² M_J at 100 K, and 3.0×10⁻³ M_J at 200 K. The S(0) line flux sets the limit at 50 and 100 K, whereas the S(1) line flux sets the limit at 200 K. The S(2) line does not set useful limits at these low temperatures, where it is very weak. Note that assuming long Spitzer integrations that set H₂ S(1) flux limits of order ∼ 10⁻²² W cm⁻², the minimum H₂ mass detectable at 40 pc via the S(1) line is 3 × 10⁻⁵ M_J, achieved when the gas is T ∼ 1020 K (see Eq. 2). Equations (1 and 2) simply relate the flux in an H₂ line to the mass of gas at a particular temperature. In the following section, we apply much more sophisticated models which actually calculate the temperature distribution in a disk, and relate the fluxes to the total mass of gas distributed in the disk.

4.2. Thermal/Chemical Modeling of Gas and Dust

4.2.1. Dust modeling

The Spectral Energy Distribution (SED) obtained from existing data in the literature and new Spitzer observations (see Figure 1) has been modeled using the dust disk models of Wolf & Hillenbrand (2003). The initial dust disk model for HD105 was presented in M04 and we only give a brief description of these previous results here. The observed infrared continuum excess cannot be uniquely fit by any one particular dust model but by a range of dust parameters. M04 assumed for simplicity that the dust is composed of astronomical silicates with a surface density distribution $\Sigma(r) \propto r^0$. The model fits were relatively insensitive to the exponent in the radial density distribution and the outer disk radius $r_{o,dust}$, since much of the dust emission at wavelengths shorter than the peak emission arises from dust near the inner radius, $r_{i,dust}$. A grain size distribution of $n(a) \propto a^{-s}$ with $s = 3.5$ was chosen, representative of regions with grain shattering, and providing somewhat better fits to the data than a single grain size. With such a distribution, most of the dust mass is in the largest particles, while the source of the infrared emission derives from grains with the minimum size a_{min} (which holds most of the dust area). We define “dust” to be particles with sizes less than $a_{max} = 1$ mm, and this definition sets the dust mass for a model fit. The three main parameters which determine the fit to the observed SED are then

the inner radius $r_{i,dust}$, the minimum grain size a_{min} , and the dust mass M_{dust} . Roughly speaking, for a given $r_{i,dust}$ and a_{min} , the dust mass sets the total solid angle subtended by dust grains, and therefore sets the ratio L_{IR}/L_{bol} of the dust IR luminosity to the stellar bolometric luminosity (an observed quantity which then determines the dust mass). M04 found acceptable fits with $r_{i,dust} = 32$ AU and $a_{min} = 8 \mu\text{m}$, and with $r_{i,dust} = 45$ AU and $a_{min} = 5 \mu\text{m}$. These best fit $r_{i,dust}$ and a_{min} corresponded to dust masses of 9×10^{-8} and $4 \times 10^{-7} M_{\odot}$.

Since the results presented in M04, we have performed a more extensive parameter study of the best χ^2 fit, and have found that the minimum in χ^2 corresponds to even larger $a_{min} = 21 \mu\text{m}$ and lower $r_{i,dust} = 19$ AU than explored in M04, and to somewhat lower dust mass $\sim 7.5 \times 10^{-8} M_{\odot}$. We found that quite good fits could be obtained for $13 \text{ AU} < r_{i,dust} \lesssim 45 \text{ AU}$. The inner dust radius cannot be smaller than 13 AU because the dust becomes too hot, and produces excess emission at $\lambda \lesssim 35 \mu\text{m}$. We do not emphasize this SED fitting procedure here because we have found, and show below, that for all acceptable dust models, there is too little dust surface area to affect the gas chemistry, heating, or cooling. Therefore, the gas spectrum is independent of the dust in the case of HD 105, and mainly depends on $r_{i,gas}$ and the gas surface density Σ_0 at $r_{i,gas}$, as we discuss below.

4.2.2. Gas/dust disk models

We apply the thermal/chemical disk models of Gorti & Hollenbach (2004) to study HD 105. In these models, a central star and the interstellar radiation field illuminate a gas and (optically thin) dust disk extending from r_i to r_o . The gas and dust are heated by the radiation field (the gas is particularly sensitive to the UV and X-ray radiation), and the gas and dust temperatures are calculated in separate thermal balance equations. The vertical density structure and chemistry is self-consistently computed by imposing thermal balance, steady-state chemistry and pressure equilibrium. The assumption in the dusty regions is that the gas and small dust particles are well mixed, so that their density ratio does not vary vertically (no settling of small dust particles). However, as we shall show, there is so little dust in HD 105 that the gas emission lines do not depend on the dust vertical (or radial) distribution. We consider various gas heating sources such as gas-dust collisions, X-rays, stellar and interstellar FUV radiation, and exothermic chemical reactions. The cooling is mainly by molecular rotational and atomic and ionic fine structure emission. In summary, the inputs to the model include the stellar parameters, the interstellar field, r_i and r_o , the surface density distribution of the gas, the dust size distribution, and the dust-to-gas mass ratio (which often is held fixed). Our main input variable generally is the gas surface density

distribution. The output is the vertical density, chemistry, and temperature distribution as a function of r , and the resultant line intensities of various ionic, atomic and molecular species. In turn, these line intensities can be compared with line observations to constrain the physical parameters in the disk, such as the gas surface density distribution (or in this case provide upper limits of gas surface densities).

We first consider a standard case, our best fit dust distribution discussed in §4.2.1, with $r_{i,gas} = r_{i,dust} = 19$ AU, i.e., *gas and dust co-exist spatially*. However, we have found in this standard case, and in other SED-fitting cases we have tested with co-existing dust where $r_{i,dust} = 13 - 45$ AU, that the dust has no effect on the gas properties. There is too little surface area to appreciably affect the cooling (through gas-dust collisions), the heating (through the grain photoelectric mechanism), or the H_2 chemistry (through catalysis of H_2 on grain surfaces). Therefore, we have also considered a number of other models with different $r_{i,gas}$, but we have not included dust since its effect is minimal.

As we shall show in the next section, the line fluxes from the gas originate from the inner regions, $r_{i,gas} < r < r_{w,gas}$, where $r_{w,gas}$ is defined such that 90% of the line luminosity is generated from $r_{i,gas}$ to $r_{w,gas}$. Considerable (gas) opacity to the stellar photons occurs at $r_{i,gas}$, so that $r_{w,gas}$ is typically only slightly ($\sim 10\%$) larger than $r_{i,gas}$, leaving the shielded outer gas beyond $r_{w,gas}$ cold and unemissive. Therefore, there can be very large amounts of cold gas in these outer regions, depending on the gas outer radius. The small amount of emission from this cold gas is below Spitzer line flux constraints. The IRS on Spitzer, however, is very sensitive to the warm gas just between $r_{i,gas}$ and $r_{w,gas}$. Because the emitting region has such small radial extent, we assume the gas surface density $\Sigma_{gas}(r) = \Sigma_0$ is a constant, independent of r *in the emitting region*. We then vary Σ_0 and compute the line fluxes. The observed line flux limits are then used to constrain Σ_0 and the gas mass M_w between $r_{i,gas}$ and $r_{w,gas}$.

If the gas extends far beyond $r_{w,gas}$, the total mass of the gas in the disk can be estimated from

$$M_{gas} = \frac{2\pi\Sigma_0 r_{i,gas}^2}{2 - \alpha} \left[\left(\frac{r_{o,gas}}{r_{i,gas}} \right)^{2-\alpha} - 1 \right] \quad \text{for } \alpha < 2, \quad (3)$$

where the gas surface density is given by $\Sigma_{gas}(r) = \Sigma_0(r_{i,gas}/r)^\alpha$ for $r_{i,gas} < r < r_{o,gas}$. Generally, α is assumed to be $\sim 0-1.5$. Note that for $\alpha < 2$ and $r_{o,gas} \gg r_{i,gas}$, considerable cold (hidden) gas mass is located at the outer radius $r_{o,gas}$.

The gas emission line fluxes then depend on only two main parameters, $r_{i,gas}$ and Σ_0 , in the case of HD 105 where dust does not affect the gas properties. The line fluxes vary with these parameters for the following reasons. X-rays and UV photons tend to penetrate and heat a fixed column of gas. Therefore, larger inner holes increase the mass of gas relative to

the total disk mass that is affected by X-ray and UV photons. However, at the same time, the stellar radiation flux falls as $1/r^2$ and the flux incident on the inner edge of the disk decreases as $r_{i,gas}$ increases. The total energy intercepted by the disk does not vary appreciably with changing $r_{i,gas}$, because the scale height tends to scale as r so that the gas disk subtends a fairly constant solid angle. However, the declining flux means a drop in the gas temperature (for fixed density), and the relative strengths of emission lines change. Similarly, Σ_0 controls the gas density at $r_{i,gas}$, and increasing Σ_0 changes the gas temperature and the relative strengths of the lines. We note that at small enough $r_{i,gas}$ the lines will become undetectable by Spitzer regardless of Σ_0 . This arises because the mass and surface area of the emitting gas decline with $r_{i,gas}$. Optically thin LTE line luminosities are proportional to mass, while optically thick lines are proportional to the emitting area. At very small $r_{i,gas}$ and when Σ_0 is raised to extremely high values, the lines cannot exceed their (optically thick) blackbody limits, the temperature is finite, and the small surface area and mass drive the beam diluted fluxes below detectability.

We consider in the next section a range of $r_{i,gas}$ from 0.5 to 100 AU. We have chosen cases of 13, 19 and 45 AU because they correspond to the minimum, the best fit, and an approximation of the maximum $r_{i,dust}$ allowable from the SED modeling. However, we also consider the possibility that the gas does not co-exist with the dust. In each case, we vary Σ_0 and determine the variation in the line fluxes with Σ_0 at the specified inner radius.

5. Results and Discussion

5.1. Gas Disks with Inner Holes

We first discuss the results of the standard case where we have included the best fit dust population and $r_{i,gas} = r_{i,dust} = 19$ AU. Figure 4 shows that model line luminosities initially increase as the gas mass surface density increases at the inner radius. The flux from the [SiII] line is the strongest followed by the [SI], [FeII], and the H₂ S(1) line. The [SiII] and [SI] lines are seen to plateau at high surface densities as they reach their optically thick, blackbody limits and as Si⁺ begins to recombine at high density. The dotted lines give the corresponding Spitzer upper limits presented in Table 1. The intersection of the (dotted line) upper limits with the (solid line) model curves for a given species marks the critical column density $\Sigma_{0,crit}$ above which the line should have been detected. With this particular choice of $r_{i,gas}$, the line providing the strongest constraint is the [SI] line, which gives $\Sigma_{0,crit} \simeq 0.14$ gm cm⁻².

It is instructive to look at the details of a fiducial model (the standard case at the critical

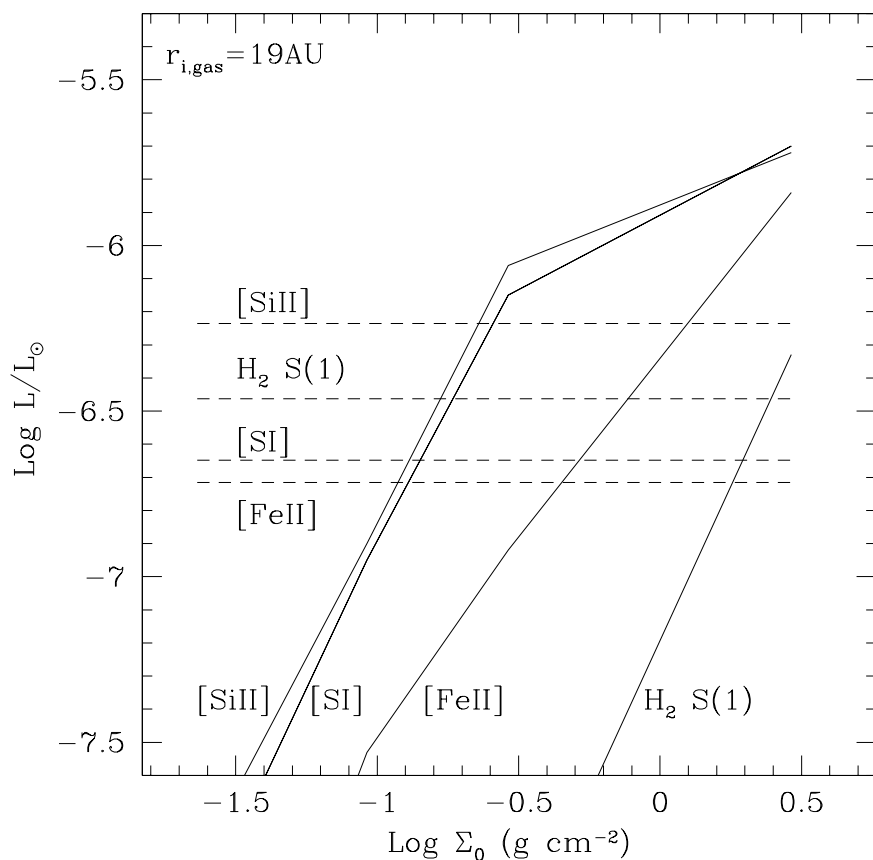


Fig. 4.— Calculated line luminosities (solid lines) as a function of gas surface density at the inner radius ($r_{i,gas} = r_{i,dust} = 19$ AU) for the strongest lines obtained for the standard model disk with the best fitting dust to the SED. The dashed lines show observed upper limits on the line luminosities as presented in this paper. Where the dashed lines meet the solid lines for a given transition marks the upper limit to the gas surface density $\Sigma_{0,crit}$ in the disk as constrained by that transition. In this case, [SI] sets the tightest constraint of $\Sigma_{0,crit} = 0.14$ gm cm⁻².

surface density for that case, $\Sigma_{0,crit} = 0.14 \text{ gm cm}^{-2}$) to understand the typical chemistry, temperature structure, and heating and cooling agents. The upper left panel of Figure 5 shows the gas temperature and the temperature of the smallest ($a_{min} = 21 \mu\text{m}$) dust grains at the midplane as a function of r . The gas density at $r_{i,gas}$ in the midplane is about 10^9 cm^{-3} . We have suppressed the data from 19 AU to 19.04 AU (a region where the gas goes from predominantly atomic hydrogen to mostly molecular hydrogen and where soft, $\sim 0.5 \text{ keV}$ X rays are absorbed), because of complicated behavior there which cannot be discerned at this graphic resolution. This small region does not significantly contribute to the line spectrum, since most of the emission arises from the much greater mass of gas that lies between 19.04 AU and 22 AU. At the inner disk edge (19 AU, not shown), the gas is atomic and fairly warm ($\sim 500 \text{ K}$), but it very quickly cools to about 150 K at 19.04 AU because of the rapid rise in abundance of cooling molecular species such as CO. One sees that beyond 19.04 AU the temperature drops from $\sim 150 \text{ K}$ to about 70 K at 22 AU. The chemistry changes slowly in this region. The hydrogen is mostly H_2 , formed by the reaction of H with H^- and on grain surfaces. We have found that eliminating grains does not change the H_2 abundance appreciably (it is nearly entirely molecular anyway). The atomic H abundance is quite high because of the inefficiency of the H^- and grain processes. Most of the sulfur is atomic, most of the silicon and iron is singly ionized. The carbon is mostly in CO, and all remaining gas phase oxygen is in atomic O. Note that when $r = 19.1 \text{ AU}$, there is already a column $N \sim 10^{22} \text{ cm}^{-2}$ of hydrogen between the central star and that point. Because the densities are very high, and the UV field low, there is considerable H_2 , C, CO, S, Si, and Fe in the surface regions, and their column provides considerable opacity to the stellar UV photons via photoionization and photodissociation processes. The dust surface area per hydrogen atom is small, so that dust extinction is not important, and the opacity is entirely due to gaseous species. Similarly, the grain surface area is too small to effectively heat the gas by the grain photoelectric heating mechanism, or to heat or cool the gas by gas-grain collisions. The gas-grain cooling could not be shown in the lower right panel because it is many orders of magnitude below the graph. We have also run alternate SED-fitting models of allowable $r_{i,dust}$ and found that dust is not important in HD 105 for modeling the gas in the disk because of its low abundance and surface area.

The main heating mechanisms for the gas in the emission zone are the heating by gaseous absorption of X-rays from the central star and of the stellar optical and UV photons which photoionize and photodissociate atoms, ions and molecules. The lower energy X-ray photons are absorbed nearest to the surface and, because of their higher cross sections for absorption, lead to the highest X-ray heating there. The more energetic X-rays penetrate further, and provide gas heating at greater depths. In the bulk of the emissive zone, the heating by optical and UV photons is dominated by the photoionization of S (which provides most of

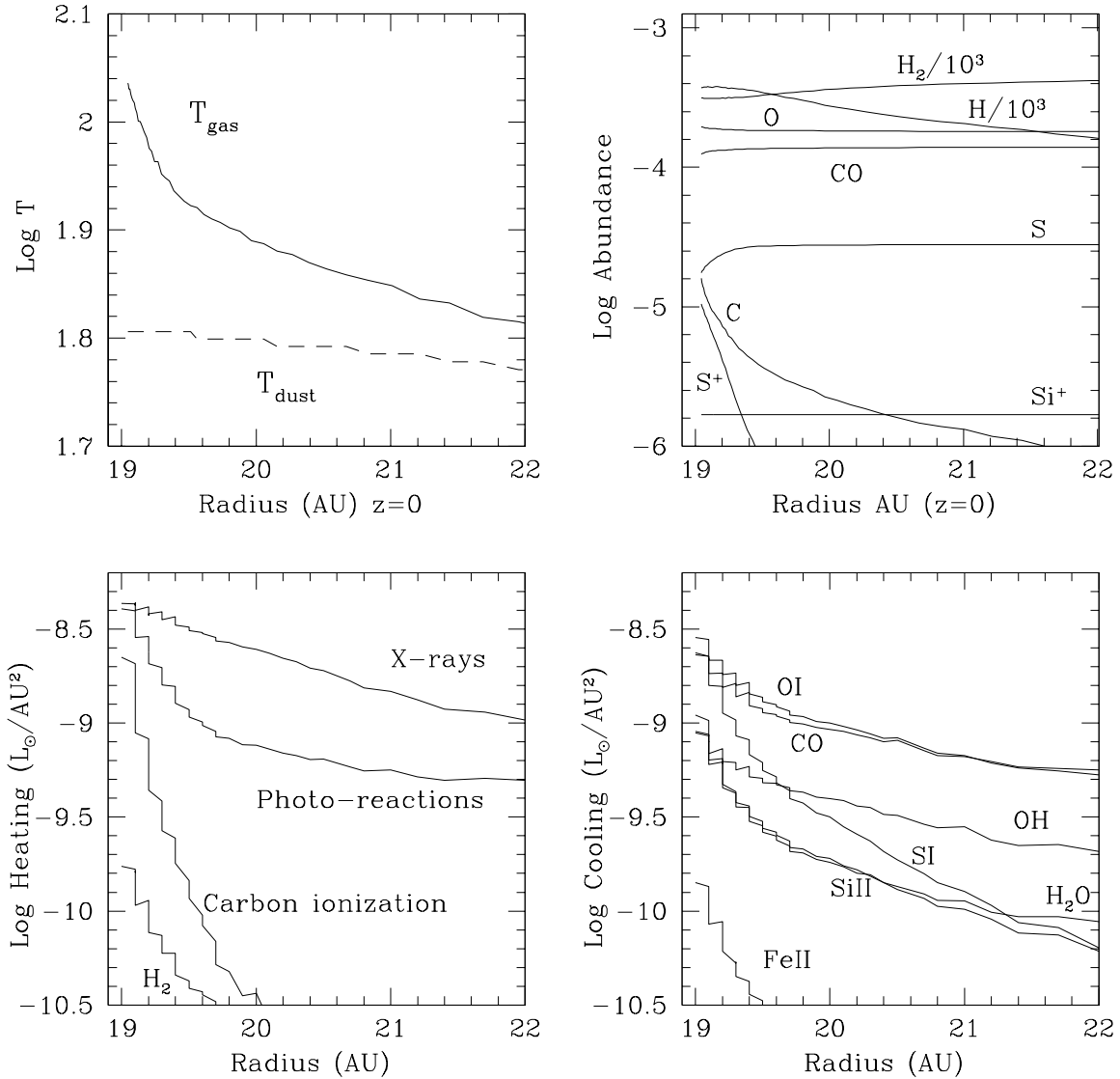


Fig. 5.— The midplane gas and a_{min} dust temperature, the midplane abundances of the abundant coolants, the total vertically integrated disk heating, and total vertically integrated disk cooling for each species as a function of radius for the emission region extending from $r_{i,\text{gas}}=19$ AU to somewhat beyond $r_{w,\text{gas}}$. We have suppressed the data from 19 AU to 19.04 AU for clarity, as discussed in the text.

the electrons) and the photodetachment of electrons from H^- . Note that this latter process requires only stellar optical photons and not the higher energy UV photons. However, this process requires H^- ; the H^- is produced by electrons which arise from the photoionization of S and Si; and these photoionizations do require UV photons. The cooling is mainly by CO mid J rotational transitions ($\sim 200 - 400 \mu\text{m}$), [SI] $25 \mu\text{m}$, and [OI] $63 \mu\text{m}$. Beyond 22 AU, the cooling is dominated by CO mid J transitions, as the gas cools below 70 K. If the gas disk extends much beyond 30 AU, these CO transitions become detectable if the CO does not freeze onto the cold grain surfaces. To date, no CO observations of HD 105 have been made. We note that the cooling by CO and [OI] occurs at longer wavelengths ($\lambda > 38 \mu\text{m}$) than accessible by the IRS on Spitzer, but that these transitions may be detectable by instruments on the future Stratospheric Observatory for Infrared Astronomy (SOFIA) and by the Herschel Observatory.

Direct heating of the gas by absorption of stellar photons heats the gas to $T \gtrsim 70\text{K}$ in the inner regions (19-22 AU) of the gas disk. The gas vertical scale height is proportional to $T^{1/2}$, and the warm gas intercepts about 20% of the stellar radiation due to its flared nature. In many wavelength bands the gas opacity is significant. Therefore, there is significant heating by this mechanism, but it tends to occur at the inner rim ($r_{i,gas}$), where the stellar fluxes are highest and least attenuated by the gas. The heating at the inner rim makes it expand vertically, enhancing its ability to intercept photons and to shield the outer disk. Dullemond, Dominik & Natta (2001) have discussed this effect for dusty disks where the opacity is provided by the dust particles. We find in the fiducial case that heated region extends radially about 3 AU beyond $r_{i,gas}$ to $r_{w,gas} \simeq 22$ AU. Of order 90% of the luminosity of the infrared lines studied here is emitted in this narrow annulus. Because of this fact, the gas spectra from the model disks around HD 105, where dust plays no factor, depend only on $r_{i,gas}$ and the gas surface density Σ_0 there, as discussed above.

We now present the results of an identical search of Σ_0 parameter space for a variety of $r_{i,gas}$ from 0.5 to 100 AU, assuming dust is unimportant. Table 2 lists the surface density limits $\Sigma_{0,crit}$ as determined from each line. Associated with each of these lines and $\Sigma_{0,crit}$ are particular values for r_w and M_w , the mass of the warm gas between $r_{i,gas}$ and r_w . These are also listed in Table 2 for the most sensitive line. Note that the warm gas masses are somewhat less than the simple analytic expression given in §4.1 for H_2 lines produced in $T \sim 100$ K gas. Spitzer can detect masses somewhat smaller than $10^{-2} M_J$ in HD 105 (the limit derived from H_2 S(1) for $T \sim 100$ K gas) because other lines such as [SI] are predicted to be stronger, and, in the cases of small $r_{i,gas}$, the gas is warmer than 100 K.

The total mass of gas (warm and cold) in any given model depends on the power law of the gas surface density distribution α and on the outermost extent $r_{o,gas}$ of the gas. Let us

Table 2: M_w , $r_{w,gas}$, and $\Sigma_{0,crit}$ as derived from the observations and models

$r_{i,gas}$ (AU)	0.5	1.0	5.0	13.0	19.0	45.0	100.0
r_w (AU)	0.69	1.28	5.15	16.5	21.9	48.6	123.0
$\Sigma_{0,crit}$ (g cm ⁻²) H ₂ S(1)	–	–	251.10	2.30	1.82	6.39	2.98
$\Sigma_{0,crit}$ (g cm ⁻²) [FeII]	6.12	2.32	0.92	0.45	0.45	0.42	1.31
$\Sigma_{0,crit}$ (g cm ⁻²) [SI]	3.43	0.36	0.12	0.11	0.14	0.21	1.04
$\Sigma_{0,crit}$ (g cm ⁻²) [SiII]	121.30	21.4	9.35	0.26	0.23	0.41	2.02
Log M_w (M _J)	-3.57	-4.09	-4.19	-2.41	-2.22	-1.61	0.6

assume that the region of gas giant formation extends to about 40 AU, based on the solar system example. We take one of the more extreme values of the power law of the gas surface density distribution, $\alpha = 0$, which maximizes the gas mass in the outer shielded zones. The upper limit (derived from the most sensitive line [SI]) to the total gas mass in this extreme case of low α is then about 1.9 M_J for $r_{i,gas} = 0.5$ AU, 0.2 M_J for $r_{i,gas} = 1$ AU, and 0.1 M_J for $r_{i,gas} = 5 - 20$ AU, where we basically extrapolate the upper limit on the gas surface density measured at $r_{i,gas}$ to 40 AU. *Therefore, for $r_{i,gas} \gtrsim 0.5$ AU, there is insufficient gas in HD 105 at this time to feed the formation of gas giants.*

Table 2 shows that the upper limits to the gas surface density at $r_{i,gas}$ are not very sensitive to $r_{i,gas}$ for $1 \text{ AU} \lesssim r_{i,gas} \lesssim 40 \text{ AU}$. Larger $r_{i,gas}$ tends to produce more mass of gas heated by the stellar photons, but, because of the dilution of the stellar flux, also tends to lead to lower characteristic gas temperature. These effects counterbalance each other to some extent, resulting in similar line fluxes.

However, for $r_{i,gas} < 1$ AU, $\Sigma_{0,crit}$ rises steeply. The heating mechanisms only penetrate to a relatively constant column of $N_w \sim 10^{22} \text{ cm}^{-2}$ so the mass of heated gas scales roughly as $r_{i,gas}^2$, assuming the vertical scale height scales with radius. Therefore, the mass (or area for optically thick lines) of heated gas goes down as we move inward, and so the gas temperature must rise appreciably in order for the gas to be detected. Since the gas temperature tends to rise with increasing density, due to the collisional de-excitation of the upper levels of cooling transitions, we require substantially more surface density to raise the temperature sufficiently to overcome the loss of warm gas mass and area.

Figure 6 visually shows how the critical surface density $\Sigma_{0,crit}$ depends on $r_{i,gas}$. We see that [SI] 25 μm is the most sensitive Spitzer line for constraining the gas surface density in gas disks with little dust, like HD 105. If $r_{i,gas}$ is sufficiently small ($\lesssim 0.5$ AU), the gas mass in the disk is essentially unconstrained by the Spitzer observations because a very small mass

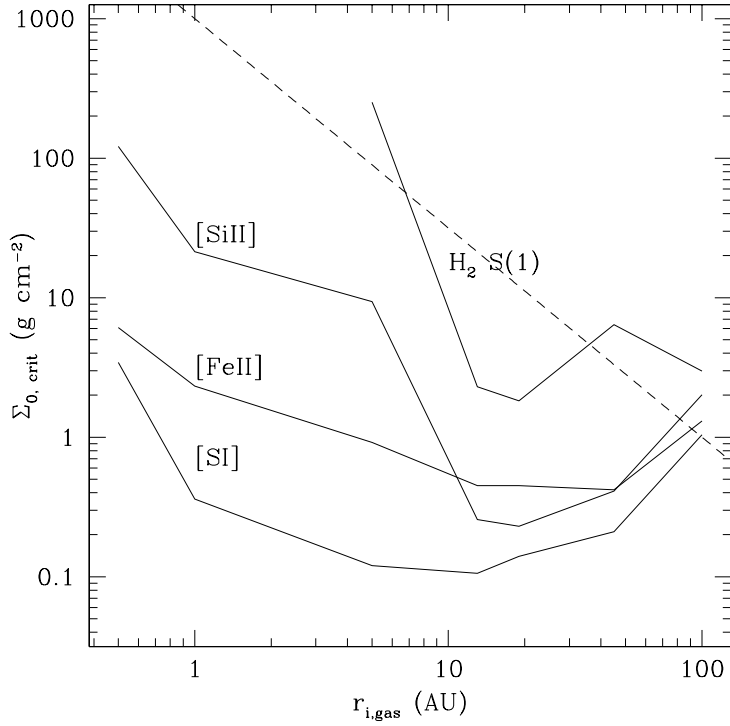


Fig. 6.— The detectable surface density based on Spitzer observations of HD 105 for a gas disk with various inner radii, and with the small amount of dust implied by the infrared continuum SED. For small $r_{i, \text{gas}} \lesssim 1$ AU, the lines set poor or no limits, as the warm emissive gas gets too optically thick and beam diluted to be detectable by Spitzer, regardless of the magnitude of Σ_0 (see text). Also shown for comparison is the surface density distribution of the minimum mass solar nebula with radius, $\Sigma(r) = 1000r_{AU}^{-3/2}$ g cm $^{-2}$ (dashed line).

and surface area of inner gas shields the outer regions, leaving them too cold to be detected at this time. Clearly, if a line detection is made by Spitzer IRS, knowledge of the parameter $r_{i,gas}$ is extremely helpful if the line flux is to be converted into $\Sigma_{0,crit}$ and M_w . Therefore, followup observations by higher spectral resolution instruments will be very useful, since resolved line widths can be translated into Keplerian velocities and, hence, $r_{i,gas}$.

5.2. Discussion

Assuming that $r_{i,gas} \gtrsim 0.5$ AU, the Spitzer upper limits to the gas lines fluxes in [SI] 25 μm , [SiII] 35 μm , [FeII] 26 μm , and H₂ S(1) 17 μm provide upper limits to the gas surface density at $r_{i,gas}$ which would indicate less than a Jupiter mass of gas is present in the gas giant planet-forming zone which extends to 40 AU. It is interesting that the most sensitive indicators of gas are not the H₂ lines, but fine structure lines (in particular [SI] 25 μm) of less abundant species (see Gorti & Hollenbach 2004). These upper limits indicate that in this region of possible gas giant planet formation, either a giant planet has already formed or it never will: *the era of significant gas accretion onto protoplanets is over for this 30 Myr old system.*

The main caveat is that if the gas surface density distribution, unlike the dust, extends to the innermost regions ($r_{i,gas} < 0.5$ AU) of the disk, then significant (i.e., $> 1 M_J$) amounts of cold gas could be hidden in the 5-40 AU region where gas giant planets may still be accreting, without violating our observational constraints on the line luminosities. However, if the gas indeed extends to < 0.5 AU, then the gas is likely accreting onto the stellar surface. If M_d is the mass of gas from the stellar surface to 40 AU, then the accretion rate onto the central star is given $\dot{M} \simeq 3 \times 10^{-9} (\alpha/0.01) (M_d/M_J) M_\odot \text{ yr}^{-1}$, where α is the standard alpha viscosity parameter. Such high accretion rates would produce diagnostics, such as large UV or near-IR excesses, H α emission lines, or other indicators of accretion-driven winds, which are not observed. Therefore, we regard this possibility as unlikely.

The gas limits in the 10-40 AU region may also be relevant to theories of the formation of the outer giants such as Neptune and Uranus. A generic problem for these systems is that they heat dynamically (i.e., induce high random velocities) the much smaller objects which provide potential coalescent collisions that enable them to grow. The higher velocities reduce the gravitational focusing, and therefore reduce their growth rate (Levison and Stewart 2001). Without some kind of dynamical cooling mechanisms, it is difficult for them to form in situ within the lifetime of the solar system. Gas drag is one possibility, but it requires many Jupiter masses of gas. Our upper limits on the amount of gas indicate that, after 30 Myr in HD 105, there is not nearly enough gas drag to have an appreciable effect (see, e.g., Goldreich

et al. 2004) at this time.

Takeuchi and Artymowicz (2001), Klahr & Lin (2001), and Takeuchi & Lin (2002) showed that a small amount of gas (and the effect of stellar photons on the gas and dust) can sculpt the dust morphology and create an inner hole. Therefore, the sharp inner dust hole at ~ 19 AU in HD 105 need not reflect the presence of giant planets, but may be produced in a planet-less gas/dust disk around HD 105. These authors show that $M_{gas} > 1 - 10M_{dust}$ produces such effects, and that when $M_{gas} > 100M_{dust}$ the dust grains cannot migrate effectively relative to the gas. Using our upper limits for the case where the gas and dust are co-spatial, we find that we can only constrain the gas mass to dust mass ratio in HD 105 to values of < 1000 , and that therefore we cannot effectively constrain the effects of gas on the dust dynamics. In other words, the sharp inner rim of dust implied by the IR continuum SED of HD 105 could be produced by a small amount of gas below our upper limits. An alternate hypothesis is that in the absence of gas, a giant planet is preventing dust from the outer debris disk from reaching the inner part of the system, as discussed in M04.

Kominami & Ida (2002, 2004) and Agnor & Ward (2002) discuss the effects of a small amount of gas in the terrestrial zone (1-5 AU) on the resulting formation of terrestrial planets. If $M_{gas} \gg 10^{-2} M_J$ in the terrestrial zone for tens of millions of years, then lunar and Mars-sized planetary embryos feel the dynamical friction of the gas, circularize their orbits, and never collide to form Earth-mass planets. On the other hand, if $M_{gas} \ll 10^{-2} M_J$, then the embryos are on eccentric orbits, and collide to form Earth-sized or larger orbits, but with eccentricities substantially larger than the Earth. The suggestion is that the Earth may have formed with roughly $10^{-2} M_J$ of gas in the terrestrial zone for tens of millions of years. The terrestrial zone ($\sim 0.3 - 3$ AU) in HD 105 is inside $r_{i,dust}$ and is currently quite dust-free. Our models show that if the gas extends all the way in to $r_{i,gas} < 0.5$ AU, then we are not sensitive to gas mass in the terrestrial zone, and therefore cannot set useful limits on this process. If for some reason the gas had an inner radius of $0.5 - 1$ AU, we can set limits of about 2×10^{-2} to $2 \times 10^{-3} M_J$ for the mass of gas from this inner radius to 5 AU. In this case, the limits are close to the critical value of $10^{-2} M_J$, and indicate perhaps insufficient gas to prevent large, Earth-sized planets from forming. Spitzer may be able to set even more stringent limits on this process in other sources. If sufficient small dust is mixed with the gas in the terrestrial zone, then the gas in the models is hotter, and smaller gas masses can be detected.

Finally, are these upper limits surprising in the context of theoretical calculations that have been performed on the likely dispersal mechanisms of the gas? The current kinematic evidence suggests that HD 105 formed in a small group of tens of stars (see §2), which likely lacked O or early B-type stars. Assuming that HD 105 was not exposed to high UV fluxes

from nearby massive stars, the main dispersal mechanism for the outer disk would likely be photoevaporation of the gas by the central star, and for the inner disk viscous accretion and spreading of the gas would dominate (Hollenbach, Yorke & Johnstone 2000, Clarke et al. 2001, Matsuyama et al. 2003). Unfortunately, it is difficult to answer this question because of the lack of self consistent photoevaporation models which treat not just the EUV (i.e., $h\nu > 13.6$ eV) photons (see Hollenbach et al. 1994), but also the less energetic stellar photons as well as the X rays from the young central star. Gorti & Hollenbach (in preparation) are developing such models, and their preliminary results show that the less energetic photons rapidly (in less than 10 Myr) disperse the gas outside of about 30-50 AU. The EUV photons can potentially remove gas outside of about 1-5 AU, but the evolution of the EUV luminosity and the radiative transfer of these photons as they try to penetrate the protostellar winds in the early stages of star formation are not well determined. A recent paper by Alexander, Clarke & Pringle (2005) suggests rather high escaping EUV luminosities which may rapidly (< 10 Myr) remove the outer gas. Once the outer disk is removed, viscosity removes the inner gas on timescales which are roughly 0.1 Myr ($0.01/\alpha_v)(r/10$ AU), where α_v is the turbulent viscosity parameter in the standard “ α ” disks. The value of α_v is typically 10^{-2} if the Balbus & Hawley (1991) magneto-rotational instability, or MRI, is operant. The MRI instability requires a minimal level of ionization, which all our relatively low mass models meet. Assuming that MRI is active, the viscous timescales inside the photoevaporation region (which lies at $> 3 - 30$ AU) are of order $0.03 - 0.3$ Myr –extremely short! On the other hand, it is not totally certain that this instability would be fully active (Chiang, Fischer, & Thommes 2002). Therefore, we conclude that these upper limits are not surprising, but they do set constraints on the rather poorly known dispersal mechanisms.

6. Summary and Conclusions

One of the goals of the Formation and Evolution of Planetary Systems (FEPS) Spitzer Legacy project is to measure the evolution and dispersal of gas in the planet-forming regions ($\sim 0.5 - 40$ AU) of disks around solar-type stars of ages 3–100 Myr. We report here our first carefully reduced and analyzed high spectral resolution data taken by the IRS instrument on the Spitzer Space Telescope. This paper illustrates our method of modeling the data to obtain constraints on the gas surface density distribution and mass. We eventually plan to obtain data on about 40 nearby stars in this age range to look for variation with age and other stellar properties.

The data presented here are for the source HD 105, a ~ 30 Myr old G0 star at a distance of 40 pc with a known IR excess arising from a circumstellar dust disk orbiting at $r_{i,dust} \gtrsim 13$

AU. The derived upper limits to the H₂ S(0) 28 μm, H₂ S(1) 17 μm, H₂ S(2) 12 μm, [SI] 25 μm, [FeII] 26 μm, and [SiIII] 35 μm lines are given in Table 1. The H₂ upper limits directly place limits on the mass of warm gas in the disk: $M(\text{H}_2) \lesssim 4.6 M_J$ at 50 K, $3.8 \times 10^{-2} M_J$ at 100 K, and $3.0 \times 10^{-3} M_J$ at 200 K. This can be compared with the roughly $10^{-3} M_J$ of gas detected around β Pictoris, a 10-20 Myr old A5 star at a distance of about 19 pc (Brandeker et al 2004). It can also be compared with the recent UV absorption measurements and analysis of AU Mic, an M1 star in the β Pictoris Moving Group at a distance of 9.9 pc and with a similar age as β Pic (Roberge et al 2005). They find an upper limit to the H₂ mass of about $2 \times 10^{-4} M_J$. It appears that even in the inner (< 30 AU) regions not well probed by CO observations, the gas is largely dissipated in these three sources which span the age range 10-30 Myr, and which span the stellar types from M1 to A5.

Detailed thermal/chemical models of HD 105 were constructed and compared with the Spitzer observations to obtain further constraints on the gas mass and surface density. These models calculate the gas temperature, chemistry, and vertical structure self-consistently and predict line fluxes which depend largely on the gas inner radius, $r_{i,gas}$, and the gas surface density Σ_0 there. We show that most of the gas emission arises in a thin inner rim, extending from $r_{i,gas}$ to $r_{w,gas}$, heated by stellar optical, ultraviolet, and X-ray photons. The upper limits on the [SI] 25 μm and [SiII] 35 μm fine structure lines provide the strongest constraints on the gas surface density Σ_0 at the inner rim.

If the gas inner radius is comparable to the observationally constrained dust inner radius, $r_{i,dust} \gtrsim 13$ AU, we show that the Spitzer upper limits on the line fluxes limit Σ_0 to $\lesssim 0.2$ gm cm⁻² for $r_{i,gas}$ between 10 and 40 AU. In this case, the total mass of gas (cold and warm) in the planet forming region between 10 and 40 AU is constrained to be less than 0.1 M_J (assuming a constant surface density between $r_{i,gas}$ and 40 AU).

The gas may not co-exist with the dust, however. We show that even if the putative gas extends inward to $r_{i,gas} = 0.5$ AU, the Spitzer upper limits set tight constraints on the gas surface density and mass. The upper limits on the gas surface density are $\Sigma_{0,crit} = 3.43, 0.36,$ and 0.12 gm cm⁻² for $r_{i,gas} = 0.5, 1,$ and 5 AU, respectively. The total mass of gas in the gas giant planet-forming region out to 40 AU depends on how we extrapolate the gas surface density from the inner radius. If we assume a gas surface density power law $\Sigma \propto r^{-3/2}$, which is often assumed in disks, then the total gas mass in these three cases is limited to about $10^{-2}, 3 \times 10^{-3},$ and $10^{-2} M_J$, respectively. An extreme assumption, allowing for the most hidden cold gas mass, would be a constant surface density with radius. In this case, we obtain total (warm and cold) gas mass limits of 1.9, 0.2, and 0.07 M_J , respectively. In summary, assuming that $r_{i,gas} > 0.5$ AU and any reasonable gas surface density distribution, there is less than a Jupiter mass of total gas in the gas giant planet forming region out to 40

AU. Given likely temperature distributions produced in our models, Spitzer is unlikely to be able to detect *total* gas masses less than about $10^{-2} M_J$ for disks around relatively nearby ($\sim 30pc$) low mass stars.

If the gas extends to $r_{i,gas} \lesssim 0.5$ AU, the Spitzer upper limits set no useful constraints on the gas mass, because gas lines become undetectable even with extremely large gas masses. In this case, the small inner rim which absorbs the heating photons from the star has too little mass (for optically thin lines) and too little surface area (for optically thick lines) to provide detectable Spitzer emission, regardless of the magnitude of Σ_0 . The outer gas is effectively shielded from the heating photons, and significant cold gas mass could exist in the planet forming regions. We argue that this case is unlikely, however, since the gas would likely extend all the way to the stellar surface, and viscous accretion onto the central star would lead to observational diagnostics such as near infrared or UV excess, $H\alpha$ emission, and signs of winds generated by the accretion process (which are not observed).

We therefore conclude that the Spitzer upper limits imply low upper limits to the gas surface density and mass in the 0.5-40 AU region around HD 105. We also note that, like HD 105, many debris disks will have too little dust to affect the gas spectra; therefore, a similar analysis of Spitzer upper limits on line fluxes will result in similar conclusions. As discussed in §5, the limits are not sufficiently stringent to constrain the potential effects of gas on dust dynamics. They set interesting limits on the mass of gas which might affect terrestrial planet formation only in the *ad hoc* case where the inner gas radius is of order 0.5 – 1 AU. However, the limits do set interesting constraints for giant planet formation. The upper limits to the gas mass obtained here are too small to enhance the buildup of gas poor outer giants such as Uranus or Neptune, and too small to allow for gas giants to form from the gas reservoir after this time (~ 30 Myr).

We acknowledge support from NASA’s Spitzer Space Telescope Legacy program, which has supported our group, the Formation and Evolution of Planetary Systems Legacy team. We thank the rest of the FEPS team for their efforts in making the FEPS project successful, and for their help in obtaining, analyzing, and interpreting the data discussed in this paper.

REFERENCES

- Adams, F.C., Hollenbach, D., Laughlin, G., Gorti, U. 2004, ApJ, 611, 360
 Agnor, C.B., Ward, W.R., 2002, ApJ, 567, 579
 Alexander, R.D., Clarke, C.J., Pringle, J.E., 2005, MNRAS, in press
 Balbus, S.A., Hawley, J.F., 1991, ApJ, 22, 1209

- Bary, J.S., Weintraub, D.A., Kastner, J.H., 2003, ApJ, 586, 1136
- Beckwith, S.V.W., Sargent, A.I. 1996, Nature, 383, 139
- Blake, G.A., Boogert, A.C.A. 2004, ApJ, 606, L73
- Boss, A., 2003, ApJ, 599, 577
- Brandeker, A., Liseau, R., Olofsson, G., Fridlund, M. 2004, A&A, 413, 681
- Brittain, S., Retting, T., Simon, T. et al. 2003, ApJ, 588, 535
- Carpenter, J., Wolf, S., Schreyer, K., Launhardt, R., Henning, T., 2005, AJ, 129, 1049
- Carr, J., Mathieu, R., Najita, J. 2001, ApJ, 551, 454
- Chen, C.H., Van Cleve, J.E., Watson, D.M., et al. 2004, AAS, 204, 4106
- Chiang, E., Fischer, D., Thommes, E., 2002, ApJ, 546, L105
- Clarke, C.J., Gendrin, A., Sotomayor, M., 2001, MNRAS, 328,485
- Cutispoto, G., Pastori, L., Pasquini, L., de Medeiros, J., Tagliaferri, G., Andersen, J. 2003, A&A, 384, 491
- Dent, W.R.F., Greaves, J.S., Coulson, I.M. 2005, MNRAS, 359, 663
- Dullemond, C.P., Dominik, C., 2004, A&A, 421, 1075
- Dullemond, C.P., Dominik, C., Natta, A., 2001, ApJ, 389, 464
- Dutrey, A., Guilloteau, S., Prato, L., Simon, M., Duvert, G., Schuster, K., Menard, F., 1998, A&A, 338, 63
- Duvert G., Guilloteau, S., Menard, F., et al. 2000, A&A, 355, 165
- Goldreich, P., Lithwick, Y., Sari, R., 2004, ApJ, 614, 497
- Gorti, U., Hollenbach, D., 2004, ApJ, 613, 424
- Greaves, J.S., 2004 MNRAS, 351, 99
- Haisch, K.E., Lada, E.A., Lada, C.J., 2001, ApJ, 553, 153
- Henry, T.J., Soderblom, D.R., Donahue, R.A., Baliunas, S.L., 1996, AJ, 111, 439
- Herczeg, G.J., Linsky, J.L., Valenti, J.A., Johns-Krull, C.M., Wood, B.E., 2002, ApJ, 572, 310
- Hillenbrand, L., Strom, S.E., Calvet, N., Merrill, M.K., Gatley, I., Makidon, R.B., Meyer, M.R., Skrutskie, M.F., 1998, AJ, 116, 1816
- Hogerheijde, M., Johnstone, D., Matsuyama, I., Jayawardhana, R., Muzerolle, J. 2003, ApJL, 595, 101

- Hollenbach, D.J., Johnstone, D., Lizano, S. Shu F., 1994, ApJ, 428, 654
- Hollenbach, D.J., Yorke, H.W., Johnstone, D. 2000, Protostars and Planets IV, 404
- Houck, J. R., Roellig, T.L. et al. 2004, ApJS, 154, 18
- Houk, N., 1978, Michigan Catalogue of HD stars
- Hubickyj, O., Bodenheimer, P., Lissauer, J.J., 2004, Rev. Mex. de Astron. y Astrop., 22, 83
- Johnstone, D., Hollenbach, D.J., Bally, J. 1998, AJ, 116, 293
- Kessler-Silacci, J.E., Hillenbrand, L.A., Blake, G.A., Meyer, M.R., 2005, ApJ, in press
- Klahr, H.H., Lin, D.N.C., 2001, ApJ, 554, 1095
- Kominami, J., Ida, S., 2002, Icarus, 157, 43
- Kominami, J., Ida, S., 2004, Icarus, 167, 231
- Kornet, K., Bodenheimer, P., Rozyczka, M., 2002, A&A, 396,977
- Lecavalier des Etangs, A., Vidal-Madjar, A., Roberge, A., et al. 2001, Nature, 412, 706
- Levison, H.F., Stewart, G.R., 2001, Icarus, 153, 224
- Lissauer, J., 1993, ARA&A, 31, 129
- Mamajek, E., Meyer, M., Hinz, P., Hoffmann, W., Cohen, M., Hora, J. 2004, ApJ, 612, 496
- Matsuyama, I., Johnstone, D., Hartmann, L., 2003, ApJ, 582, 893
- Metanomski, A.D.F., Pasquini, L., Krautter, J., Cutispoto, G., Fleming, T.A., 1998, A&AS, 131, 19
- Meyer, M.R. et al. 2004, ApJS, 154, 422
- Meyer, M.R. et al. 2005, in preparation.
- Miyake, K., Nakagawa, Y., 1993, Icarus, 106, 20
- Najita, J., Carr, J., Matheiu, R. 2003, ApJ, 589, 931
- Natta, A., Testi, L., Neri, R., Shepherd, D., Wilner, D. 2004, 416, 179
- Perryman, M.A.C., et al. 1997, A&A, 323L, 49
- Pietu, V., Dutrey, A., Kahane, C., 2003, A&A, 398, 565
- Pollack, J., Hubickyj, O., Bodenheimer, P., 1996, Icarus, 124, 62
- Przygodda, F., van Boekel, R., Abraham, P. et al. 2003, A&A, 412, L43
- Qi, C., Kessler, J.E., Koerner, D.W., Sargent, A.I., Blake, G.A., 2003 ApJ, 597, 986
- Randich, S., Pallavicini, R., Meola, G., Stauffer, J., Balachandran. S. 2001, A&A, 373, 862

- Rettig, T.W., Haywood, J., Simon, T., Brittain, S.D., Gibb, E., 2004, ApJ, 616, 163
- Richter, M., Jaffe, D.T., Blake, G.A., Lacy, J.H., 2002, ApJ, 572, 161
- Roberge, A., Weinberger, A.J., Redfield, S., Feldman, P.D. 2005, ApJ, in press.
- Sako, S., Yamashita, T., Kataza, H., Miyate, T., Okamoto, Y.K., Honda, M., Fujiyoshi, T., Onaka, T. 2005, ApJ, 620, 347
- Sheret, I., Ramsey Howat, S.K., Dent, W.R.F. 2003, MNRAS, 343L, 65
- Silverstone, M. 2000, PhD Thesis
- Soderblom, D.R., Oey, M.S., Johnson, D.R.H., Stone, R.P.S. 1990, AJ, 99, 595
- Skrutskie, M.F., Snell, R., Dutkevitch, D., Strom, S.E., Schloerb, F.P., Dickman, R.L., 1991, AJ, 102, 1749
- Suttner, G., Yorke, H.W., 2001, ApJ, 551, 461
- Takeuchi, T., Artymowicz, P. 2001, ApJ, 557, 990
- Takeuchi, T., Lin, D.N.C., 2002, ApJ, 581, 1344
- Testi, L., Natta, A., Shepherd, D.S., Wilner, D.J., 2003, A&A, 403, 323
- Thebault, P., Augereau, J-C. 2005, A&A, in press
- Thi, W.F., van Dishoeck, E.F., Blake, G.A., van Zadelhoff, G.J., Horn, J., Becklin, E.E., Mannings, V., Sargent, A.I., van den Ancker, M.E., Natta, A., Kessler, J., 2001, ApJ, 561, 1074
- Thi, W.-F., van Dalen, B., Bik, A., Waters, L.B.F.M., 2005, A&A, 430, 61
- Throop, H.B., Bally, J., Esposito, L.W., McCaughrean, M.J., 2001, Science, 292, 1686
- van Boekel, R., Waters, L.B.F.M., Dominik, C., Bouwman, J., de Koter, A., Dullemond, C.P., Paresce, F., 2003, A&A, 400, 21
- van Dishoeck, E.F., 2004, ARA&A, 42, 119
- Weinberger, A., Becklin, E., Zuckerman, B., Song, I. 2004, AJ, 127, 2246
- Weidenschilling, S.J., Spaute, D., Davis, D.R., et al. 1997, Icarus, 128, 429
- Weidenschilling, S.J. 1977, MNRAS, 180, 57
- Werner, J. R., et al. 2004, ApJS, 154, 1
- Wolf, S., Hillenbrand, L.A., 2003, ApJ, 596, 603
- Wolf, S., Padgett, D., Stapelfeldt, K.R., 2003, ApJ, 588, 373
- Wichmann, R., Schmitt, J., Hubrig, S. 2003, A&A, 399, 983

Zuckerman, B., Forveille, T., Kastner, J.H. 1995, *Nature*, 373, 494